nature astronomy

Article

https://doi.org/10.1038/s41550-023-02104-8

Observation of the Mars O_2 visible nightglow by the NOMAD spectrometer onboard the Trace Gas Orbiter

Received: 27 March 2023

Accepted: 18 September 2023

Published online: 09 November 2023

Check for updates

J.-C. Gérard[1] ✉, L. Soret[1], I. R. Thomas[2], B. Ristic[2], Y. Willame[2], C. Depiesse[2], A. C. Vandaele[2], F. Daerden[2], B. Hubert[1], J. P. Mason[3], M. R. Patel[3] & M. A. López-Valverde[4]

On Mars, atomic oxygen controls the carbon dioxide radiative cooling of the upper atmosphere and the presence of an ozone layer near the poles. To remotely probe meridional transport of O atoms from the summer to the winter hemisphere and the descending flow in the winter polar regions, the O_2 Herzberg II atmospheric emission could be used as a proxy. This emission is quite weak on Earth's nightside, but it is prominent in the Venus night airglow, and it has not previously been observed on Mars. Here we report the limb detection of the O_2 Herzberg II visible bands in the Mars nightglow with the NOMAD ultraviolet–visible spectrometer onboard the European Space Agency's Trace Gas Orbiter. The emission layer reaches up to hundreds of kilorayleighs in the limb viewing geometry. It is mainly located between 40 km and 60 km at high latitudes during the winter season, consistent with three-body recombination of oxygen atoms. This O_2 nightglow should be observable from a Martian orbiter as well as from the Martian surface with the naked eye under clear sky conditions. These observations pave the way to future global observations of the Martian atmospheric circulation with simpler lower-cost instrumentation.

The mesosphere of Venus and Mars is still poorly known as data are scarce and global circulation models can hardly reproduce them. Its composition, circulation pattern and variability are still not well understood. It is important to characterize the Martian upper atmosphere to determine the structure of the terrestrial planets' atmospheres and understand their different evolution. Observations of airglow emissions is a powerful remote-sensing tool that provides insight into the density variations and global transport in this region.

The Mars airglow emissions on the dayside have been extensively studied based on observations performed with instruments onboard the Mariner, Mars Express (MEx), Mars Atmosphere and Volatile Evolution Mission (MAVEN), Trace Gas Orbiter (TGO) and Emirates Mars Mission (EMM). Following the first observations from the Mariner 6 and 7 flybys[1], later studies have described the distribution of the ultraviolet CO Cameron, CO_2^+ UV doublet and Fox–Duffendack–Barker bands, H Lyman-α, O I 130 nm and 136 nm multiplets, and N_2 Vegard–Kaplan emissions, and their sources and dependence on latitude, solar longitude and solar activity. Recently, observations of the [O I] 557.7 nm and the 630–636 nm forbidden emissions made with the TGO Nadir and Occultation for Mars Discovery (NOMAD) instrument and their seasonal variability have been reported[2–5].

On the nightside, only the ultraviolet and infrared emissions have been explored with spectral instruments onboard the MEx and MAVEN missions. The middle ultraviolet spectrum is dominated by the $v' = 0$ δ and γ bands of nitric oxide excited by radiative association of nitrogen and oxygen atoms. Although this emission is present at all latitudes

[1]LPAP, STAR Institute, Université de Liège, Liège, Belgium. [2]Royal Belgian Institute for Space Aeronomy, Brussels, Belgium. [3]School of Physical Sciences, The Open University, Milton Keynes, UK. [4]Instituto de Astrofisica de Andalucía/CSIC, Granada, Spain. ✉e-mail: jc.gerard@uliege.be

https://doi.org/10.1038/s41550-023-02104-8

and local times, extensive mapping has shown that it is enhanced at high winter latitudes in both hemispheres[6]. This brightening is a consequence of the transport of O and N atoms from the summer to the winter hemisphere where they are carried downwards by vertical winds and diffusion and recombine in the 40–60 km region. The O_2 infrared atmospheric band at 1.27 μm[7–9] and the OH Meinel emission at 1.45 μm and 2.9 μm[10] have also been measured in the Martian polar winter atmosphere over a similar range of altitudes. They also result from meridional transport and winter polar descent of O atoms produced by photodissociation of CO_2 in the summer hemisphere.

No nightglow spectrum has been observed so far in the visible domain. Scattered solar light hinders such measurements from Earth's ground and no space-borne instrument has observed the Mars visible nightglow. In this Article, we describe new observations made with the ultraviolet and visible (UVIS) channel, a spectrometer of the NOMAD instrument flying on the ExoMars TGO. They cover both hemispheres, but their number is limited by operational constraints. Nevertheless, visible nightglow emissions have been observed on several TGO orbits. The observations reported here were episodically collected between March 2020 and October 2022 with the UVIS instrument. The TGO satellite has been orbiting Mars since October 2016 on a circular orbit at ~400 km, inclined 74° relative to the equator with an orbital period of ~2 h. The UVIS instrument covers the 200–650 nm spectral range and can observe in both the nadir and the solar occultation modes. The UVIS spectral resolution varies from 1.2 nm at 200 nm to 1.6 nm at 650 nm[11,12]. For the observations described in this study, the TGO spacecraft was oriented so that the line of sight of the nadir channel was pointing in the limb direction[13]. Two pointing modes were used during this period. In the first one, 'inertial pointing', the line of sight was kept fixed in the inertial space so that the line of sight scanned a range of altitudes usually from 300 km, down to 40 km, then up to 300 km. In the second one, most frequently used in this study, the areoid altitude of the tangent point in the atmosphere remained within ~20 km of a pre-set value while different latitudes were probed due to the motion of the spacecraft. The spectra were integrated over 20 s. The resolution at the tangent point, taking into account the UVIS field of view during the spectral integration provided a vertical resolution of 10 ± 5 km.

The NOMAD-UVIS instrument occasionally collected limb spectra during nightside conditions, with solar zenith angles greater than 105° at the tangent point of the line of sight. A band structure clearly appeared in some individual bright spectra between 400 nm and 600 nm. The wavelengths and relative intensities indicate coincidence with the strongest bands of the $v' = 0$ progression of the O_2 $c^1\Sigma_u \rightarrow X^3\Sigma_g$ Herzberg II transition[14].

A total of 1,228 spectra were acquired between 20 km and 70 km and with a solar zenith angle >105°, out of which 122 were kept (Methods). The average spectrum is shown in Fig. 1. The (0,5) to (0,11) Herzberg II bands are clearly identified with relative intensities similar to those observed on Venus[15] and in the laboratory[16]. Beyond 620 nm, the noise level increases, making detection of the (0,12) band uncertain. The total intensity for bands $v' = 5$ to $v' = 12$ derived from the spectral fit combined with the relative band intensity in the laboratory is 108 ± 11 kR. The estimated error combines contributions from the absolute calibration and measurement noise including the uncertainty in the spectral baseline.

The confirmed spectral detections spread over 13 orbits are shown in Fig. 2. A first group of detections extends from 50° S to 81° S when the solar longitude L_s varied from 94° to 158°. A second one covers the L_s range 225–330° between 65° N and 81° N. The mean spectrum is shown in Fig. 1.

The observed wavelengths perfectly match those in the laboratory and Venus Herzberg II spectra. The small differences in relative band brightness in Fig. 1 result from the presence of the background noise level in the UVIS data. The relative band intensities in the brightest individual spectra show excellent agreement of the spectral shape.

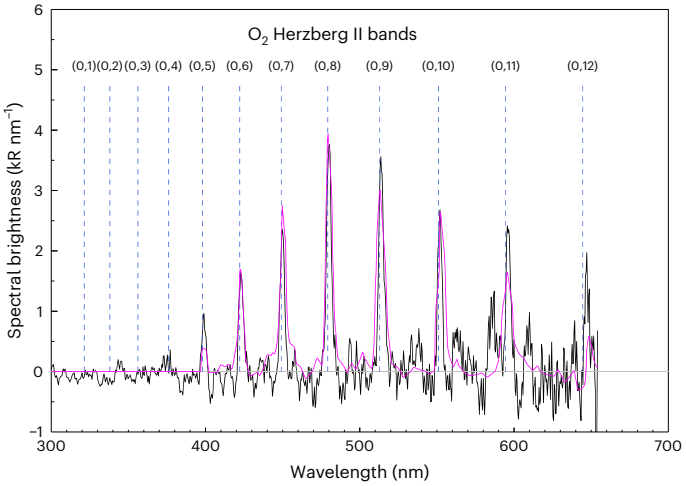

Fig. 1 | Average high-latitude nightglow spectrum. The identifications of the $v' = 0$ Herzberg II bands are indicated by the vertical dashed lines. The purple curve is the reference Venus nightglow spectrum scaled to the UVIS mean spectrum. A total of 122 high-latitude NOMAD-UVIS spectra have been averaged (black curve).

There is no indication of a departure of the intensity distribution compared with the Venus or laboratory spectra. By analogy with the Venus nightglow spectrum, the presence of other weak O_2 band systems, such as the Chamberlain $A'^3\Delta_u \rightarrow a^1\Delta_g$, Herzberg I $A^3\Sigma_u \rightarrow X^3\Sigma_g$ and $c^1\Sigma_u \rightarrow a^1\Delta_g$ bands, may be expected in the region of the (0–6) to (0–12) Herzberg II bands. On Venus, their contribution is about 7%, 5% and 4% of the Herzberg II intensity, respectively[15]. However, the signal-to-noise ratio of the UVIS instrument is clearly too low to confirm their presence in the UVIS nightglow spectra.

In Fig. 2, inertial limb detections are represented with dots and limb tracking observations are shown with triangles. Each dot colour corresponds to one TGO orbit. Grey symbols represent observations without detection. Figure 2a illustrates the concentration of the detections under high-latitude winter conditions. Figure 2b indicates that the visible nightglow is observed between 34 km and 66 km, generally polewards of 60°. The statistics of the detections are too small to obtain a statistically significant mean limb profile.

Figure 3a shows the histogram of the altitudes of the spectra binned into 1 km intervals corresponding to a positive detection at the linear Pearson correlation coefficient $R > 0.32$ level. A maximum of 35 detections is observed at 42 km. The brightest single spectrum reached an intensity of 290 kR at 41 km and 76° N. The detection lower limit for single 15 s spectra is on the order of 20 ± 10 kR. Figure 3b presents the histogram of the detection relative frequency of occurrence versus altitude. They are mainly grouped between 35 km and 59 km. The highest value is also observed at 42 km where the occurrence is a large as 76%. The detection frequencies at higher altitudes remain below 10%.

The detection of the visible Herzberg II bands in the Mars dayglow makes its measurement a promising technique to derive the atomic oxygen density and its variations in the middle atmosphere. It is produced by three-body recombination of atomic oxygen, following the scheme:

$$O + O + M \rightarrow O_2^* + M \quad (1)$$

where M is the atmospheric number density. This is the accepted mechanism for the excitation of the O_2 nightglow in atmospheres[17]. Models based solely on three-body recombination of O atoms have been shown to adequately explain the observed O_2 Herzberg II intensity in the Venus nightglow[18] and the O_2 $^1\Delta$ nightglow on Mars. Other processes have been mentioned as potential sources of O_2 $c^1\Sigma$ molecules

https://doi.org/10.1038/s41550-023-02104-8

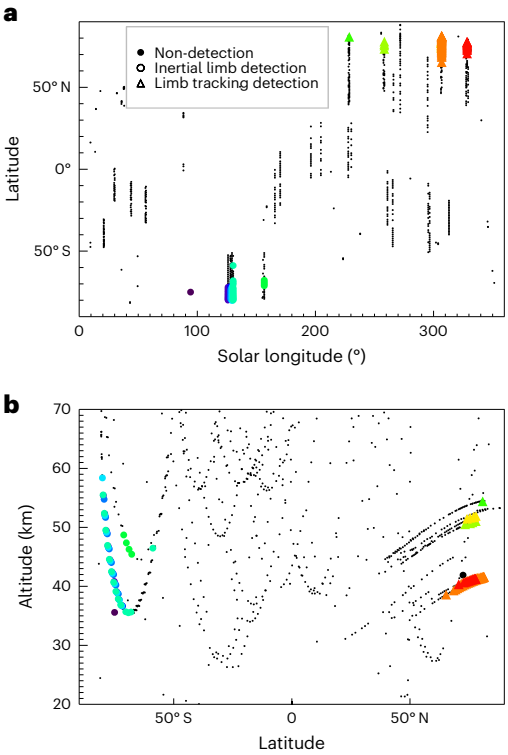

Fig. 2 | Distribution of detections of the O_2 Herzberg II nightglow. **a**, Latitude and season of the detections. **b**, Areoid altitude–latitude map of the observations. The triangles indicate limb tracking and the dots indicate inertial pointing orbits. Each dot colour corresponds to one TGO orbit. Small grey dots correspond to observations without a measurable Herzberg II spectral signature.

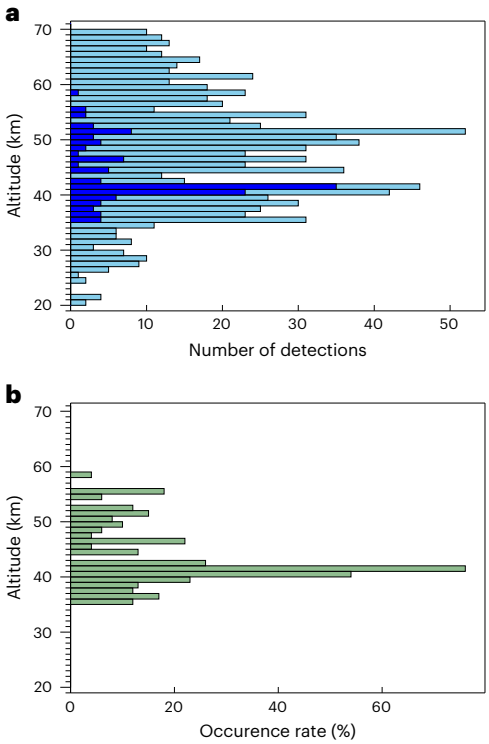

Fig. 3 | Altitude distribution of the nightside limb observations. **a**, NOMAD-UVIS observations (light blue) and positive detections (dark blue). **b**, Rate of occurrence of detections.

on Venus, but they have been considered negligible in models of the O Venus and Mars nightglow[18,19]. In the absence of evidence for other source processes, we consider process (1) as the only important source of O_2 c $^1\Sigma$ excitation.

Model simulations for a zonally averaged atmosphere have been performed for different L_s and latitudes in both hemispheres. The volume emission rate is calculated based on process (1) and the relevant Mars Climate Database (MCD) temperature and density distributions. Figure 4 shows the calculated limb profile of the brightness of the Herzberg II bands. Slightly lower values are predicted at latitudes beyond 75° but they are expected to drop considerably at lower latitudes. The calculated peak brightness decreases to a few kilorayleighs at 60° N and moves up to 58 km. For the sake of completeness, the calculated limb profile for 60° N is also shown, although no nightglow observation has been performed in the limited database. Some intensity measurements from individual spectra are also shown for comparison. They either closely agree with the model value (79° N, 76° N, 76° S) or exceed it by a factor of 2 (75° N). The measurement at L_s = 50°, 65° S has been collected in May 2023 and shows a discrepancy relative to the model by about an order of magnitude. This indicates that the O density was significantly higher than the value predicted by the MCD at the time of the observations. This difference is observed at a moderately high latitude, suggesting that the modelled meridional transport does not provide enough O atoms at these lower latitudes. If discrepancies are demonstrated to be reliable, they should provide new insights into the dynamical processes in the atmosphere, thereby improving the reliability of three-dimensional GCMs. Additional observations are necessary to confirm whether the discrepancies at these latitudes are common or occasional.

The clear spectral signature and its analogy with the laboratory and Venus nightglow, together with the general agreement of the predicted altitude and brightness, confirm that the observed spectrum is produced by three-body recombination of O atoms. The enhanced brightness at high latitudes is the signature of the global transport ascending from the sunlit summer polar regions and descending to the dark winter hemisphere.

The O_2 $a^1\Delta_g \rightarrow X^3\Sigma_g$ infrared atmospheric emission at 1.27 µm is another recombination emission also observed in the Martian nightglow. The peak altitude of the emitting layer varies between 40 km and 65 km reaching up to 12 MR at 40 km in both winter regions at latitudes beyond ~70°[7–9]. In the case of the $a^1\Delta_g$ metastable state, the recombination efficiency of the O atoms is on the order of 70% and collisional deactivation is negligible at the altitude of the emitting layer. Consequently, the intensity of the infrared atmospheric system is about 60 times higher than the Herzberg II bands.

Collisions between O and CO_2 in the thermosphere populate the vibrational levels of CO_2, resulting in enhanced radiation of the 15 µm emission to space and atmospheric cooling[20]. Consequently, the O density governs the efficiency of the non-local thermodynamic equilibrium (non-LTE) radiative cooling in the upper atmosphere. Although this process essentially occurs at higher altitude than most of the O_2 airglow emission, the O peak density derived from the nightglow vertical profile may be used to constrain the O density at higher altitudes. Therefore, the determination of its distribution and variability is of prime importance in understanding and modelling the thermal structure of the Martian upper atmosphere. Transport of O atoms across the terminator also has a key role as a precursor in the formation of an ozone layer near the south winter pole[21].

Future measurements will allow better determination of the emission peak altitude, its brightness and variability. They will provide unique constraints on three-dimensional models of the global circulation[22] and dynamical processes at play in the middle atmosphere. By accumulating nightside limb observations, it will be possible to describe the mean O density distribution at high winter latitudes and

https://doi.org/10.1038/s41550-023-02104-8

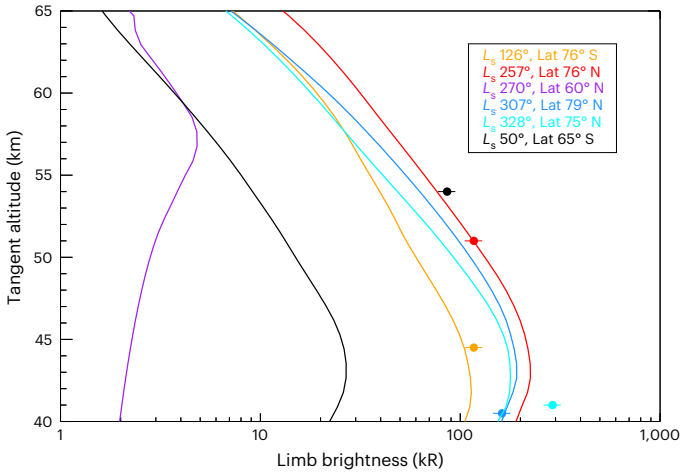

Fig. 4 | Model simulations of the limb brightness distribution of the O_2 Herzberg II bands. The simulated limb profiles are calculated from expression (2) (Methods) based on densities and temperature from the MCD for different latitudes and seasons. The circles indicate UVIS observations using corresponding colours. The observed intensity values are: 117 kR, 45 km (orange); 117 kR, 51 km (red); 162 kR, 40 km (blue); 290 kR, 41 km (cyan); 86 kR, 54 km (black). The error bars are estimated at 10% of the brightness. No detection at latitudes as low as 60° N is available in the current database.

its variability. In particular, additional observations will determine how accurately the transition of the bright nightglow from one hemisphere to the other is predicted by three-dimensional models. The question of a possible hemispheric asymmetry in the spatio-temporal airglow distribution will also be examined based on a larger number of detections.

The brightness of the O_2 Herzberg bands of several hundred kilorayleighs in the visible opens the possibility to observe them in the Martian high-latitude regions with simple space-borne cameras in the visible domain. We also note that the sensitivity threshold of the human eye in the green for nightside vision is estimated on the order of 1 kR[23], decreasing at shorter and longer wavelengths[24]. For the Herzberg bands, which are widespread over most of the visible range, a likely wavelength-averaged threshold value is on the order of a few kilorayleighs, much lower than the bright emission described in this report. The polar winter visible nightglow is therefore expected to be observable with the naked eye by future astronauts from orbit or the Martian ground. Incidentally, we note that the oxygen green line at 557.7 nm is not observed in UVIS bright individual spectra nor after co-addition of nightglow spectra (Fig. 1). This non-detection sets an upper limit of about 1 kR on the line brightness. It is in full agreement with its absence in the laboratory recombination spectra and the lack of detection by the Mars 5 visible spectrometer setting an upper limit of 50 R[19] on the nightglow limb brightness of the green line.

Methods

Data processing

During the pipeline processing of the spectra, the instrumental background and the dark current on the charge-coupled device (CCD) frame are first removed. In a second step, the noise is corrected from cosmic rays, anomalous and hot pixels. Next, the 81 fully illuminated CCD lines are binned to increase the signal-to-noise ratio of the individual spectra. In a third step, the count rate is converted into physical units (kilorayleighs, 1 kR corresponds to a brightness of 10^9 photons per square centimetre per second emitted in 4π steradians), using laboratory measurements and in flight calibration[25]. In addition to the statistical error on the count rate and removal of the background noise, a possible systematic error of ~10% is associated with the uncertainties of the absolute instrumental calibration.

For verification of positive spectral detections, we calculate the correlation coefficient between the individual NOMAD spectra and the Venus nightglow average spectrum[26], between 410 nm and 560 nm at a resolution of 3 nm. This Venus reference spectrum was obtained by summing nightglow spectra collected between 92 km and 100 km with the Visible and Infrared Thermal Imaging Spectrometer (VIRTIS-M) on board Venus Express during a total of 120 h[26]. The Venus reference spectrum has been scaled to the UVIS averaged spectrum, following a least-squares fit. NOMAD-UVIS spectra with a linear correlation coefficient $R > 0.32$ have been retained and those with a too low signal-to-noise ratio have been removed. Application of the statistical Fisher test indicates that this correlation coefficient is significantly different from zero with a confidence level of 99%. A subsequent visual examination identified a number of contaminated spectra that have been removed from the database.

Model simulations

The volume emission rate of the band system based on process (1) is given by:

$$\eta(O_2) = \varepsilon K[O]^2[M]\frac{A}{A + k_{CO2}[CO_2] + k_O[O]} \quad (2)$$

where $[M]$ is the total number density, and $[O]$ and $[CO_2]$ are the O and CO_2 densities from the MCD; $\varepsilon = 0.03$ is the effective yield of the $c^1\Sigma_u$ state including cascades from higher lying states; $A = 0.17\ s^{-1}$ is the total transition probability of the c–X transition, that is, from $(c, v' = 0)$ to all (X, v'); $K = 7.5 \times 10^{-33}\ (T/300)^{-3.25}$ is the total recombination coefficient of the three-body recombination of O in CO_2; $k_{CO2} = 3.1 \times 10^{-16}\ cm^{-3}\ s^{-1}$ and $k_O = 5.9 \times 10^{-12}\ cm^{-3}\ s^{-1}$ are the quenching coefficients of the $c^1\Sigma_u$ state by CO_2 and O, respectively.

We adopt values deduced from the studies of the Venus airglow[19] based on laboratory measurements[17] and Venus Express observations[26,27]. They have been slightly adapted to match the O_2 nightglow limb observations with the VIRTIS spectral imager[28,29]. The K coefficient and its temperature dependence are adopted from ref. 30. The recombination rate is multiplied by 2.5 to account for the higher efficiency of CO_2 relative to N_2 as a third body[31]. For comparison with our observations, the O and CO_2 densities are taken from the MCD version 6.1[32] for minimum solar activity conditions. Limb profiles are calculated by integrating the volume emission rate along the line of sight.

Data availability

The NOMAD-UVIS spectra can be downloaded from ESA's SA archives at https://archives.esac.esa.int/psa/#!Table%20View/NOMAD=instrument (select UVIS from the list of instruments and 'Level 3 Calibrated' from the processing level). Observed limb intensities and model calculations supporting Fig. 4 are available from BIRA-IASB repository at https://doi.org/10.18758/71021084 or from the corresponding author upon reasonable request.

References

1. Barth, C. A. et al. Mariner 6 and 7 ultraviolet spectrometer experiment: upper atmosphere data. *J. Geophys. Res.* **76**, 2213–2227 (1971).
2. Gérard, J. C. et al. Detection of green line emission in the dayside atmosphere of Mars from NOMAD-TGO observations. *Nat. Astron.* **4**, 1049–1052 (2020).
3. Gérard, J. C. et al. First observation of the oxygen 630 nm emission in the Martian dayglow. *Geophys. Res. Lett.* **48**, e2020GL092334 (2021).
4. Aoki, S. et al. Density and temperature of the upper mesosphere and lower thermosphere of Mars retrieved from the O I 557.7 nm dayglow measured by TGO/NOMAD. *J. Geophys. Res.* **127**, e2022JE007206 (2022).

5. Soret, L. et al. The Mars oxygen visible dayglow: a Martian year of NOMAD/UVIS observations. *J. Geophys. Res.* **127**, e2022JE007220 (2022).
6. Schneider, N. M. et al. Imaging of Martian circulation patterns and atmospheric tides through MAVEN/IUVS nightglow observations. *J. Geophys. Res.* **125**, e2019JA027318 (2020).
7. Bertaux, J. L., Gondet, B., Lefèvre, F., Bibring, J. P. & Montmessin, F. First detection of O_2 1.27 μm nightglow emission at Mars with OMEGA/MEX and comparison with general circulation model predictions. *J. Geophys. Res.* **117**, E00J04 (2012).
8. Fedorova, A. et al. The O_2 nightglow in the martian atmosphere by SPICAM onboard of Mars-Express. *Icarus* **219**, 596–608 (2012).
9. Clancy, R. T. et al. Extensive MRO CRISM observations of 1.27 μm O_2 airglow in Mars polar night and their comparison to MRO MCS temperature profiles and LMD GCM simulations. *J. Geophys. Res.* **117**, E00J10 (2012).
10. Clancy, R. T. et al. First detection of Mars atmospheric hydroxyl: CRISM near-IR measurement versus LMD GCM simulation of OH Meinel band emission in the Mars polar winter atmosphere. *Icarus* **226**, 272–281 (2013).
11. Patel, M. R. et al. NOMAD spectrometer on the ExoMars trace gas orbiter mission: part 2—design, manufacturing, and testing of the ultraviolet and visible channel. *Appl. Opt.* **56**, 2771–2782 (2017).
12. Vandaele, A. C. et al. An integrated suite of three spectrometers for the ExoMars trace gas mission: technical description, science objectives and expected performance. *Space Sci. Rev.* **214**, 1–47 (2018).
13. López-Valverde et al. Investigations of the Mars upper atmosphere with ExoMars Trace Gas Orbiter. *Space Sci. Rev.* **214**, 29 (2018).
14. Krupenie, P. H. The spectrum of molecular oxygen. *J. Phys. Chem. Ref. Data* **1**, 423–534 (1972).
15. Krasnopolsky, V. A. in *Venus* (eds Hunten D. M. et al.) 459–483 (Univ. Arizona Press, 1983).
16. Lawrence, G. M., Barth, C. A. & Argabright, V. Excitation of the Venus night airglow. *Science* **195**, 573–574 (1977).
17. Slanger, T. G. & Copeland, R. A. Energetic oxygen in the upper atmosphere and the laboratory. *Chem. Rev.* **103**, 4731–4766 (2003).
18. Bougher, S. W. & Borucki, W. J. Venus O_2 visible and IR nightglow: implications for lower thermosphere dynamics and chemistry. *J. Geophys. Res.* **99**, 3759–3776 (1994).
19. Krasnopolsky, V. A. Excitation of the oxygen nightglow on the terrestrial planets. *Planet. Space Sci.* **59**, 754–766 (2011).
20. Bougher, S. W., Hunten, D. M. & Roble, R. G. CO_2 cooling in terrestrial planet thermospheres. *J. Geophys. Res.* **99**, 14609–14622 (1994).
21. Montmessin, F. & Lefèvre, F. Transport-driven formation of a polar ozone layer on Mars. *Nat. Geosci.* **6**, 930–933 (2013).
22. Forget, F. et al. Improved general circulation models of the Martian atmosphere from the surface to above 80 km. *J. Geophys. Res.* **104**, 24155–24175 (1999).
23. Omholt, A. *The Optical Aurora* (Springer, 1971); https://doi.org/10.1007/978-3-642-46269-6
24. Lilensten, J. Prediction of blue, red and green aurorae at Mars. *Planet. Space Sci.* **115**, 48–56 (2015).
25. Willame, Y. et al. Calibration of the NOMAD-UVIS data. *Planet. Space Sci.* **218**, 105504 (2022).
26. García Muñoz, A., Mills, F. P., Slanger, T. G., Piccioni, G. & Drossart, P. Visible and near-infrared nightglow of molecular oxygen in the atmosphere of Venus. *J. Geophys. Res.* **114**, E12002 (2009).
27. García Muñoz, A. et al. Limb imaging of the Venus O_2 visible nightglow with the Venus Monitoring Camera. *Geophys. Res. Lett.* **40**, 2539–2543 (2013).
28. Gérard, J. C., Soret, L., Migliorini, A. & Piccioni, G. Oxygen nightglow emissions of Venus: vertical distribution and collisional quenching. *Icarus* **223**, 602–608 (2013).
29. Migliorini, A. et al. The characteristics of the O_2 Herzberg II and Chamberlain bands observed with VIRTIS/Venus Express. *Icarus* **223**, 609–614 (2013).
30. Smith, G. P. & Robertson, R. Temperature dependence of oxygen atom recombination in nitrogen after ozone photolysis. *Chem. Phys. Lett.* **458**, 6–10 (2008).
31. Nair, H., Allen, M., Anbar, A. D., Yung, Y. L. & Clancy, R. T. A photochemical model of the Martian atmosphere. *Icarus* **111**, 124–150 (1994).
32. Millour, E. et al. The Mars Climate Database (Version 6.1). *EPSC Abstr.* **16**, EPSC2022-786 (2022).

Acknowledgements

B.H. is research associate of the Belgian Fund for Scientific Research (FNRS). ExoMars is a space mission of ESA and Roscosmos. The NOMAD experiment is led by the IASB-BIRA, assisted by co-principal-investigator teams from Spain (IAA-CSIC), Italy (INAF-IAPS) and the United Kingdom (The Open University). This project acknowledges funding from BELSPO, with the financial and contractual coordination by the ESA Prodex Office (PEA grant numbers 4000140863, 4000121493 and 4000129683). M.A.L.-V. was supported by grant number PGC2018-101836-B-100 (MCIU/AEI/FEDER, EU) and CEX2021-001131-S funded by MCIN/AEI/10.13039/501100011033. We also acknowledge support from the UK Space Agency through grant numbers ST/V002295/1, ST/V005332/1, ST/Y000234/1 and ST/X006549/1'. We thank the ESA TGO team and its project scientists H. Svedhem and C. Wilson for supporting these observations.

Author contributions

J.-C.G. and L.S. conceived the study and wrote the paper. Y.W., C.D., I.R.T. and J.P.M. calibrated the UVIS data and prepared the datasets. Observation planning was managed by J.-C.G., L.S., B.R., and M.R.P. A.C.V. is the NOMAD principal investigator, M.R.P. is NOMAD co-principal investigator. All authors contributed to discussion and comments on the paper.

Competing interests

The authors declare no competing interests.

Additional information

Correspondence and requests for materials should be addressed to J.-C. Gérard.

Peer review information *Nature Astronomy* thanks Antonio García Muñoz and Guillaume Gronoff for their contribution to the peer review of this work.

Reprints and permissions information is available at www.nature.com/reprints.

Publisher's note Springer Nature remains neutral with regard to jurisdictional claims in published maps and institutional affiliations.

Springer Nature or its licensor (e.g. a society or other partner) holds exclusive rights to this article under a publishing agreement with the author(s) or other rightsholder(s); author self-archiving of the accepted manuscript version of this article is solely governed by the terms of such publishing agreement and applicable law.

© The Author(s), under exclusive licence to Springer Nature Limited 2023